

AN ANALYTICAL APPROACH TO GAS TURBINE ENGINE MODEL LINEARIZATION

Gi-Yun Chung*
Manuj Dhingra
J.V.R. Prasad

School of Aerospace Engineering
Georgia Institute of Technology
Atlanta, GA 30332

Richard Meisner

Steven Sirica
Pratt & Whitney
East Hartford, CT 06108

ABSTRACT

This paper presents analytical linearization schemes of a reduced order aero-thermodynamic model of the generic back end of a turbofan engine. The proposed linearization scheme has advantages of flexibility and reusability over the commonly used linearization method based on the numerical perturbation scheme. Also, a blending algorithm employing the distance to the boundary as the weight has been incorporated into the linearization scheme to capture the change of the flow behaviour near bifurcating boundaries. The proposed linearization scheme is developed and applied to a back end model of a generic turbofan engine with bifurcations corresponding to choked/unchoked boundaries. This model is also used for proof of concept validation test.

NOMENCLATURE

A	matrix for linearization
A_i	Area at the i^{th} station
c_p	Specific heat at constant pressure
D_i	Distance to the boundary
K	Work extraction coefficient
p_a	Ambient pressure
p_i	Static pressure at the i^{th} station
$p_{t,i}$	Stagnation pressure at the i^{th} station
r	Rotor radius
SISO	Single Input Single Output
T_i	Static temperature at the i^{th} station
$T_{t,i}$	Stagnation temperature at the i^{th} station
u_i	Flow velocity at the i^{th} station

γ	Ratio of specific heats
η	Efficiency
ϕ	Flow coefficient
ψ	Stage loading coefficient
ω	Rotor speed

INTRODUCTION

Linear models have historically been very useful in the design and analysis of control and estimation algorithms for gas turbine engines [1]. Whereas gas turbine engines are significantly nonlinear in a large signal sense, their small signal response near equilibrium can generally be well represented by a set of local perturbation linear models. The existence and validity of such linear models enable the use of well established approaches for the design and analysis of control laws and estimators. This includes classical single input/single output control law design, multivariable control [2,3], model predictive control [4], and Kalman filter estimation [5,6]. As the accuracy and performance of controllers greatly depend on the engine model, it follows that developing an accurate model that captures the transition of different flow characteristics of entire flight envelope is the first step in designing a good engine controller.

A detailed model of the engine is usually developed to simulate the engine behavior across the entire operating envelope. Although such models are generally not usable in real time due to computational and numerical issues, they can serve as the basis of simpler, faster models targeted at control and health monitoring functions. Control oriented engine modeling methods can be broadly classified into two

* Corresponding author

categories: physics based models and data-driven black box models. Typically, a physics based approach directly models the inter-component aero-thermal properties as well as shaft dynamics while employing a map/look-up table type representation of the components [7-9]. A limited number of correlation parameters derived from test data may also be used to fill in missing information. A black-box approach may attempt to derive arbitrary mathematical functional relationships between input and output data, where the data is either obtained via experiment or simulation. Examples of this approach include state variable models, neural network based engine models, and support vector machine based engine models. In practice, a control and/or health monitoring engine model may mix these approaches. In any case, the chief motivation is to improve the accuracy while minimizing computational costs.

A judicious use of input-output data can yield a data-driven model that is more accurate than a simplified physics based model. However, the selection of training and validation data sets is a key challenge. Another unfavorable aspect is the necessity to redevelop the entire model if there is any change in even one of the engine components. Moreover, the lack of a direct correlation with underlying physics makes it difficult to diagnose any erratic behavior. A physics-based modeling approach makes it easier to relate observed behavior to the underlying processes. Not only can the engine component changes be incorporated into a physics-based model with minor modifications, the generic nature of such a model makes it applicable across a family of engine designs. A key benefit lies in the behavior of the model outside the validated domain: adherence to physical laws ensures reasonable dynamic behavior during untested operating conditions.

Design of control systems for linear systems is a well established field. As a consequence of Lyapunov's indirect method it is possible to design linear controllers that are guaranteed to be stable in the neighborhood of an equilibrium point of a non-linear system. In most current generation engine controllers, it is typical to divide the operating regime into segments or modes and design linear controllers for each of these modes. Each controller computes demanded values independent of others. The final actuator demands are calculated by an appropriate blending of different modes. There is thus a need to obtain linear models at specified operating points across the envelope of engine operation.

Given that the detailed engine model cannot be analytically represented, one way to obtain linear estimates is via numerical perturbation [10-12]. The coefficients obtained in this fashion have to be stored in onboard memory. As the system can be highly non-linear over the entire envelope, linearization has to be carried out at several operating points to achieve acceptable level of accuracy. Storage being a constrained resource, this leads to a trade-off between accuracy and memory use. Of course, any changes to the system require a recalculation of the entire set of linear coefficients.

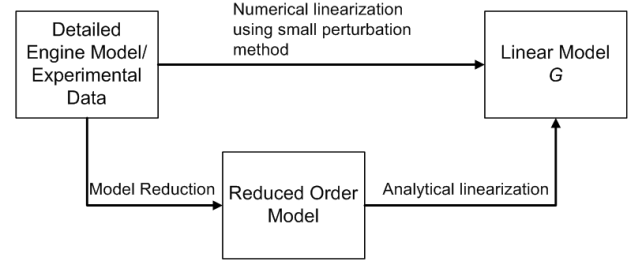


Figure 1. Different linearization approach

In the present work, the development of a reduced order model followed by analytical linearization of the resulting system is proposed as an alternative to the numerical technique [Figure 1]. The outcome is a modeling methodology that is flexible yet computationally efficient. The paper is organized in the following manner. The basic rationales for the modeling methodology are first described. This is followed by the details of a reduced order model for the back end of a turbofan engine. The key features of this non-linear system are explored via a computer simulation. The discontinuity in the slope of mass flow rate with respect to control inputs divides the domain into subspaces. Results show the validity of the linearized model in the interior of each subspace. The observed large errors in linear estimates when crossing subspace boundaries is improved via a novel blending approach. The paper concludes with future research topics.

It may be noted that the proposed methodology is illustrated via application to the back end of a turbofan. The eventual goal is to extend the model to a complete engine with shaft dynamics.

THEORETICAL RATIONALE

For a nonlinear system with slow and fast dynamics represented in terms of slow states x_1 (spool dynamics, metal temperature dynamics, etc) and fast states x_2 (flow dynamics in different components of an engine) of the form

$$\begin{aligned} \dot{x}_1 &= f_1(x_1, x_2, u) \\ \dot{x}_2 &= f_2(x_1, x_2, u) \end{aligned} \quad (1)$$

Linearization of the above equations about an equilibrium solution (x_{10}, x_{20}, u_0) results in

$$\begin{aligned} \delta \dot{x}_1 &= \frac{\partial f_1}{\partial x_1} \delta x_1 + \frac{\partial f_1}{\partial x_2} \delta x_2 + \frac{\partial f_1}{\partial u} \delta u \\ \delta \dot{x}_2 &= \frac{\partial f_2}{\partial x_1} \delta x_1 + \frac{\partial f_2}{\partial x_2} \delta x_2 + \frac{\partial f_2}{\partial u} \delta u \end{aligned} \quad (2)$$

When one considers the flow behavior in the back end of an engine, the flow dynamics may be considered to be relatively

fast, which are outside the typical bandwidth of an engine controller. Hence, the flow dynamics of such a system may be residualized, i.e., the dynamic equations associated with x_2 are treated as algebraic equations. Hence, the residualized form of the fast dynamics are given by

$$f_2(x_1, x_{2o}, u) = 0 \quad (3)$$

The sensitivity of the flow behavior to small control inputs can be analyzed using the linearized form of the above equation. It is reasonable to assume that when a control perturbation δu is applied from an equilibrium condition (x_{1o}, x_{2o}, u_o) , over the small instant of time during which the fast states x_2 reach a new equilibrium, i.e., $x_{2o} + \delta x_{2o}$, the change in slow state x_1 , from its initial equilibrium value x_{1o} , will be very small, and hence, may be neglected. Then one can use a linearized form of the above equation by treating x_1 to be same as x_{1o} for analyzing the effects of control perturbation δu on resulting flow behavior change δx_{2o} . The linearized form of the above equation becomes

$$\frac{\partial f_2}{\partial x_{2o}} \delta x_{2o} + \frac{\partial f_2}{\partial u} \delta u = 0 \quad (4)$$

Or in a matrix form,

$$\mathbf{A} \delta \underline{x} + \mathbf{B} \delta u = 0 \quad (5)$$

The focus of the following sections is to develop an analytically linearizable form of flow equations applicable to the back end part of a turbojet engine and evaluate the fidelity of the linearized equations, especially in the presence of component level flow choking due to control perturbations. Further, a novel scheme for blending of linearized models across component level choking boundaries is proposed and is evaluated.

SIMPLIFIED REPRESENTATION OF THE BACK END

As the engine goes through startup procedure, the turbine and propulsive nozzles may go from an unchoked flow regime to a choked flow regime. The choke point is a function of system geometry as well as work extracted across the turbine stages. A relevant simplified model should be able to capture the unchoked to choked transition as well as the flexibility of the turbine versus propulsive nozzle choking. The performance of a turbine stage is usually represented in terms of a map that relates outlet stagnation pressure and component efficiency to inlet stagnation pressure and mass flow rate [13-15]. One advantage of the simplified model presented here over a map type representation is the ability to explicitly capture choked-unchoked flow conditions.

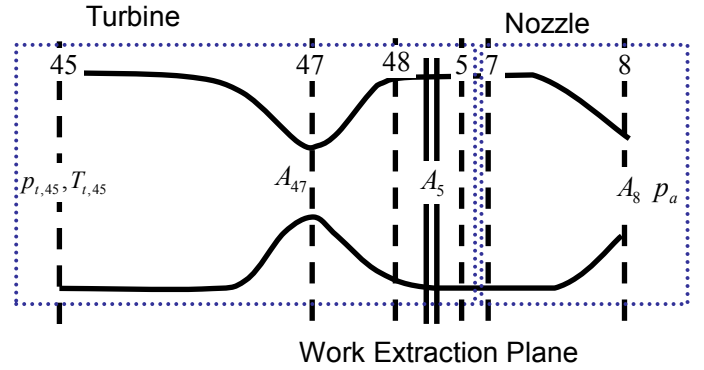


Figure 2. The proposed model description of generic back end model of a single spool turbofan

As the rotor dynamics are significantly slower than gas dynamics, following the previous section the gas dynamics can be residualized. This leads to a set of nonlinear static equation that can be solved for gas states, given rotor dynamics and control inputs. Again following the theoretical rationale, equilibrium values for the rotor state can be used to calculate the quasi-steady values of the gas states.

Turbine-Nozzle Model

In the present work, the turbine component is represented by a combination of a throat area and a work-extraction plane. The work extraction plane is not unlike the usual component map. Work and efficiency are specified as a function of the flow coefficients and formally expressed as,

$$\eta = f(\phi) \quad (6)$$

$$\psi = g(\phi) \quad (7)$$

It is assumed that flow characteristics remain on the subsonic branch of the aerodynamic solution. The flow is assumed to be isentropic with the efficiency equation encapsulating all the loss generating mechanisms.

The propulsive nozzle is modeled as a simple converging-diverging duct, a work extraction and loss generation plane, and a converging duct. This is illustrated via Figure 2. The inputs to this system are the total inlet stagnation pressure ($p_{t,45}$) and the nozzle area (A_8). The boundary conditions are given by the ambient pressure and cross-sectional areas at stations 47 and 5. The outputs of the system are mass flow rate (\dot{m}), exit velocity (u_8), total temperature after work extraction ($T_{t,50}$) and total pressure after work extraction ($p_{t,50}$).

In general, the extraction plane equation can be of any complex form. However, for the purpose of this paper, a simple yet functionally relevant relationship is assumed. The turbine efficiency is assumed to be a constant. Whereas this is not true across the engine operating envelope, it may be a valid

approximation locally. Based on the known behavior of a single stage, a linear relationship between stage loading and flow coefficient is assumed for the work extraction. With these assumptions, equations (6) and (7) yield the following equations for stagnation temperature and pressure drop across the extraction plane.

$$\Delta T_{t,45} = \frac{K\omega r}{c_p} u_{48} \quad (8)$$

$$\left(\frac{p_{t,5}}{p_{t,45}}\right) = \left[1 - \frac{1}{\eta} \left(1 - \frac{T_{t,5}}{T_{t,45}}\right)\right]^{\frac{\gamma}{\gamma-1}} \quad (9)$$

It is emphasized that these simplifying assumptions do not lead to a loss of generality. A complex work and efficiency to flow rate relationship would increase the complexity of the solution procedure used for the non-linear model simulation but would not fundamentally change the linearization process.

The simplified, physics based back-end model is described by a set of non-linear equations, included in their entirety as Appendix A.

Features of the Nonlinear System

The system of nonlinear equations representing the simplified model have been simulated via MATLAB for a range of nozzle exit area and inlet stagnation pressure inputs. The results in form of contour plots of mass flow and thrust are presented in Figures 3 and 4, respectively. The independent variables in these plots are nozzle exit area to turbine throat area ratio and inlet stagnation to outlet (ambient) pressure ratio. Contour plots have been found to be a valuable tool in the visualization of system characteristics as one or more of the input parameters are varied. The nonlinear solution is subject to bifurcation around choking of the turbine and the nozzle. Flow can either be subsonic or choked at each component level and the mass flow rate is dictated by the choked component. The contour plots clearly indicate three distinct subspaces represented by different slopes in the mass flow rate and the thrust. These subspaces are the subsonic regime, the nozzle choked regime, and the turbine choked regime as illustrated by red, blue and yellow shades, respectively. In addition, three boundaries (denoted as B1, B2, and B3 in Figures 3 and 4) representing the bifurcation in flow characteristics are superimposed on the contour to indicate when the nozzle and/or the turbine are choked.

As the engine goes through a startup procedure, the turbine-nozzle subsystem transitions from a highly nonlinear system to an essentially linear system. This transition occurs as the relationship between the mass flow rate and the pressure ratio drop across the turbine becomes linear when either the turbine or the nozzle is choked. This change in behavior is a key challenge in control design. This feature can be observed in Figure 3, the contour plot of mass flow rate. For a fixed nozzle exit area, the spacing between two consecutive contour levels is unequal on the left of the B2 boundary. When the system is operating at higher pressure ratios, to the right of this boundary, the contours are uniformly spaced, again for a fixed area ratio.

The nozzle is not the only component that is expected to choke at higher pressure ratios. If the nozzle area is much larger than the equivalent throat area of the turbine, the turbine may choke first. This boundary is represented by the curve B1 in Figure 3. Again, to the right of the boundary B1, as expected, the contour levels are uniformly spaced, relative to pressure ratio for a fixed area. The third boundary of this system, marked B3, separates turbine choked and nozzle choked subspaces. As this boundary is crossed from region 3 to region 2, due to an increase in the exit area of the variable nozzle, mass flow becomes independent of nozzle area. The overall thrust for this simplified system still has a small dependence on the nozzle area, as evident in Figure 4. This is mainly due to the continued dependence of exit velocity on the

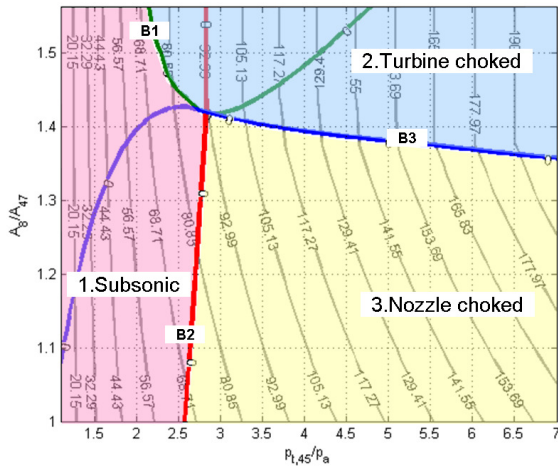


Figure 3. Mass flow rate contour plot

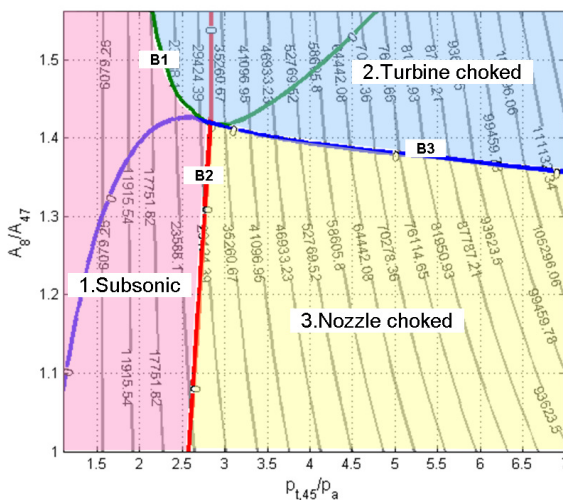


Figure 4. Thrust contour plot

nozzle area, with a minor contribution from the differential pressure.

LINEARIZATION

The solution of the nonlinear set of equations is computationally expensive. As mentioned before, sensitivity of the flow behavior to small changes in control can be computed via the linearized counterpart. The nonlinear system exhibits distinct subspaces that correspond to choking and unchoking of the various components. As the set of equations describing each subspace is different, the resulting set of linearized equation is also different for the different subspaces. These analytically linearized equations for the matrix \mathbf{A} , the matrix of linear coefficients, are included in Appendix A.

When the operating point is restricted to any one subspace, the non-linear system is smooth and hence the matrix \mathbf{A} is a continuous function of its independent variables. It is thus expected that in the interior of each subspace, the respective linear systems would yield good estimates of perturbed states for given control variations. A comparison of the non-linear simulation results to the corresponding linear system shows that this is indeed true. Figure 5 shows the results corresponding to a pressure ratio sweep. At each operating point, defined by a given area and pressure ratio, a control perturbation of a 5% increase in pressure and a 2% decrease in nozzle exit area is applied. The figure shows all the four outputs: stagnation temperature and pressure drop across the turbine component due to a change in turbine work, mass flow rate and the flow velocity at the nozzle exit plane. The error is defined as the difference in the linear estimates and the true nonlinear values of the perturbed system outputs, normalized with respect to the true values.

As long as the operating point is away from subspace boundaries, the linear estimates of the change in turbine work, mass flow rate and exit velocity match the true values. There is a large error as the system goes from subsonic to choked turbine operating conditions.

Whereas the current example corresponds to a relatively large change in the input variable, the large error near a subspace boundary is observed for any magnitude of the change. The large error region gets wider or narrower as the percentage change in control inputs is increased or decreased. Fundamentally, the error arises due to a discrete change in the linearized system equations across a subspace boundary. For a control input that leads to a subspace transition, neither set of linearized equations is strictly correct. It may be possible to mitigate the impact of this large error by limiting the permissible control changes to small values near subspace boundaries. However, a promising approach based on blending the output of multiple linearizations near the boundary has been developed as part of the current work and is presented in the following section.

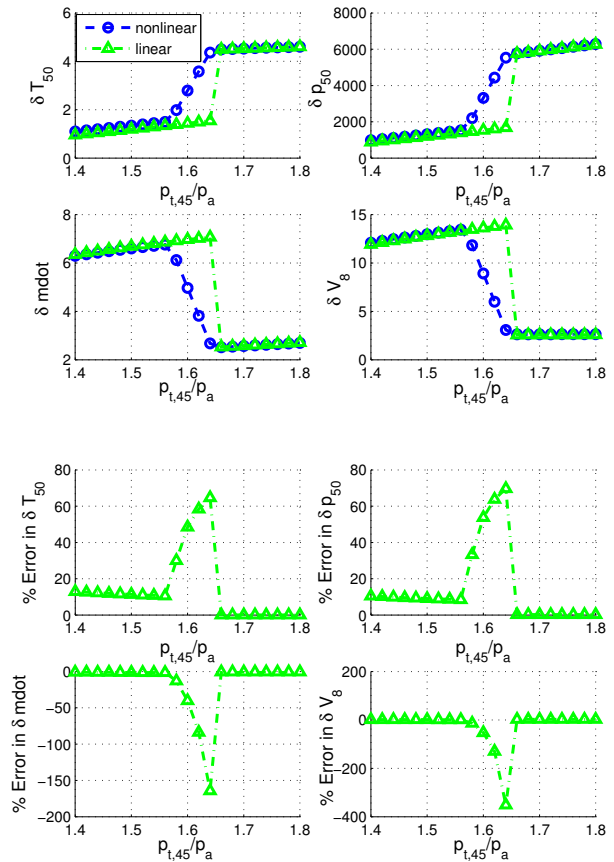


Figure 5. (a) Linear vs. nonlinear solution going from the subsonic regime to the turbine choked regime (b) % error of the linear solution

BLENDING ACROSS THE SUBSPACE BOUNDARIES

The simulation results of the non-linear representation of the turbine-nozzle system show that it has three distinct subspaces. The flow in the entire system is subsonic, the turbine is choked or the propulsive nozzle is choked. The boundaries separating the subspaces correspond to unique operating conditions in which either one or both of the components just get choked. Near the boundaries, as the results of the previous section show, the linearized estimate can strongly deviate from the true value of any of the output variables.

To mitigate this error, a strategy to detect boundary crossing has been developed here. Given that the linear models are discontinuous across subspace boundaries, the linear estimate is computed as a weighted sum of two linear estimates, one for each subspace. A key requirement to efficiently implement this blending approach is the availability of analytical expressions that define each boundary. This requirement is satisfied in this work as the analytical linearization scheme offers the analytical expressions of each

boundary. In the conventional numerical linearization scheme, it would be difficult to obtain the analytical expressions. For the turbine-nozzle subsystem used in this work, equations for each of the three boundaries are developed utilizing basic flow properties. A blending algorithm that utilizes these boundary equations to improve linear estimates near the subspace boundaries is detailed and evaluated.

The boundary between the subsonic flow (Region 1) and turbine choked (Region 2) represents the scenario where the flow through the nozzle is still completely expanded and the Mach number at the turbine throat reaches unity. When both these conditions are imposed on the general set of equations, an equation for the boundary can be written as,

$$\frac{A_{47}}{A_8} - \frac{p_{t,5}}{p_{t,45}} \sqrt{\frac{T_{t,45}}{T_{t,5}}} \left(\frac{2\gamma}{\gamma-1} \right) \left(\frac{\gamma+1}{2} \right)^{\frac{\gamma+1}{2(\gamma-1)}} \left(\frac{p_a}{p_{t,5}} \right)^{\frac{1}{\gamma}} \sqrt{1 - \left(\frac{p_a}{p_{t,5}} \right)^{\frac{\gamma-1}{\gamma}}} = 0 \quad (10)$$

This boundary is a function of the turbine work, available inlet stagnation pressure and enthalpy, as well as the geometric parameter, turbine throat to nozzle area. The nozzle area ratio essentially determines whether the nozzle or the turbine components will get choked once critical pressure ratios are reached. The boundary B2 between the subsonic flow and the nozzle choked regions represents the scenario when the pressure after the turbine is just sufficient to choke the nozzle. Again the flow is fully expanded to the ambient at the nozzle exit. The relevant analytical expression is given by:

$$\frac{p_{t,5}}{p_a} - \left(\frac{\gamma+1}{2} \right)^{\frac{\gamma}{\gamma-1}} = 0 \quad (11)$$

At the boundary of nozzle choked and turbine choked subspaces, both the components are just choked. An equation for the boundary B3 can thus be obtained by equating the choking mass flow rates through the two components. The resulting expression is

$$\frac{A_{47}}{A_8} - \frac{p_{t,5}}{p_{t,45}} \sqrt{\frac{T_{t,45}}{T_{t,5}}} = 0 \quad (12)$$

The boundary B1 and B3 share first few terms because both of them are obtained by equating the mass flow rate of the turbine choked region with mass flow rate of the nozzle either when it is choked or subsonic.

It may be noted that all the three boundaries are dependant on the turbine work. Boundary B1 and boundary B3 also depend on the nozzle to turbine throat areas. Further, each boundary has a spurious branch, which is part of the theoretical solution, but not applicable to the turbine-nozzle system. As an example, part of the boundary B1 corresponds to the supersonic solution. Similarly, for a part of boundary

B3, the available inlet pressure is lower than a critical value, and hence, neither the turbine nor the nozzle can be realistically choked. Care must be taken to neglect these spurious branches on the numerical implementation of the blending algorithm.

Blending Algorithm

The blending algorithm is a simple 2-step approach. Detect if a boundary would be crossed for a given control input and if so calculate the weights for the corresponding linear systems. In the proposed approach, both of the steps involve calculating the distance to the boundary before and after the controlled inputs are applied. Geometric considerations allow one to deduce the change of subspace; specifically the distance to the boundary must change sign when a boundary is crossed. As the contour plots show (Figure 3 and 4), the operating point may be close to multiple boundaries. The boundary most likely to be active is the one that is closest. This can either be determined from the nonlinear solution, or better directly from the boundary equations.

The availability of analytical boundary conditions allows for a quick calculation of the distance to the boundary. The distance to the boundary before the application of control perturbation can be directly calculated by evaluating the left-hand side of the relevant boundary equation. To calculate the distance after the perturbation, the variables in the boundary equation take their values from the results predicted by the linear system of equations. This implies that the distance after the perturbation is an approximation, but the results show that it provides acceptable estimates.

In Figure 6, D_1 represents the distance to the boundary before the perturbation and D_2 represents the distance to the boundary after the perturbation. If the product of D_1 and D_2 is positive then flow properties of both before and after the perturbation are located in the same region and no crossing of the boundary is detected. The boundary of interest has been crossed when the product of D_1 and D_2 is negative. When the product of the D_1 and D_2 is zero, the flow is right at the boundary and the flow characteristics are satisfied by using either Region 1 equations or Region 2 equations.

As suggested earlier, if a boundary crossing is detected, a possible solution is to reduce control step sizes to ensure that the boundary is not transgressed. However, the blended output can provide accurate linear estimates and hence deemed superior. The blended output uses the distance to the boundary as weights in a weighted average approach. As an example, blended mass flow rate can be written as

$$\dot{m} = \frac{D_1}{D_1 + D_2} \dot{m}_1 + \left(1 - \frac{D_1}{D_1 + D_2} \right) \dot{m}_2 \quad (13)$$

where the regions 1 and 2, and the distances D_1 , D_2 are as illustrated in Figure 6.

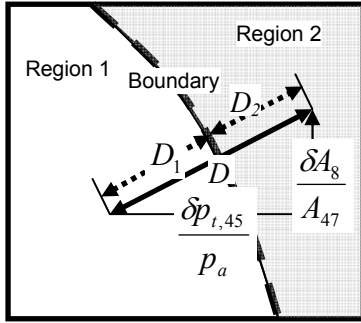


Figure 6. Description of boundary crossing

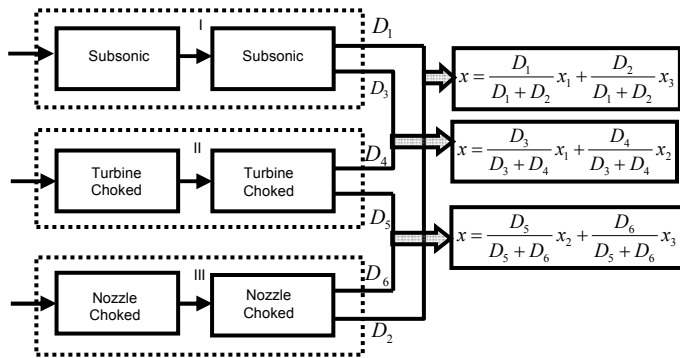


Figure 7. Blending algorithm at the boundaries

Figure 7 outlines the general structure of the blending algorithm using the weights used in this work. It is to be noted that this algorithm requires the computation of outputs in the both sub-regions for the combined answer.

The robustness and stability near the neighborhood of the boundaries are subject to more rigorous analysis. The bifurcating behavior observed is similar to the linear parameter varying dynamical system. Balas and Wolodkin et al have applied the parameter dependent control design to the turbofan engine [16,17]. The parameter dependent control is not the scope of this paper; however, in the future work, similar theoretical analysis can be applied to the current model.

The blending approach has been implemented and verified against the true, nonlinear estimate of output perturbations. The results show that this simple approach can provide significant improvements in the linear estimates near the subspace boundaries.

The results for a 5% increase in inlet pressure and a 2% decrease in nozzle exit area are presented in Figure 8. This case corresponds to the results in Figure 5 i.e., equilibrium area-ratio leads to the crossing of boundary B1 between subsonic to turbine choked subspaces. As evident from a comparison of the two figures (Figures 5 and 8) the blended results show a significant improvement over the baseline. As expected, this error decreases with a decrease in control perturbation.

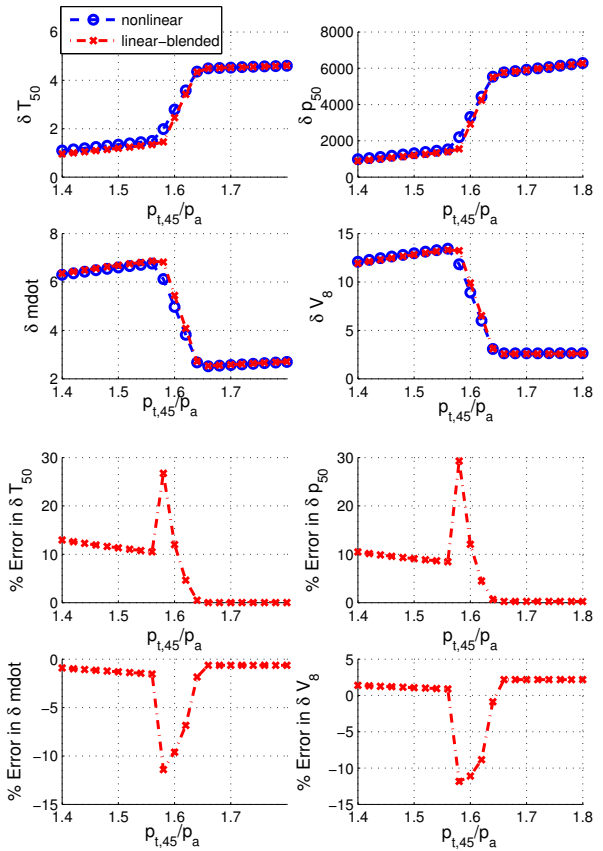


Figure 8. (a) Linear vs. nonlinear solution going from the subsonic regime to the turbine choked regime (b) % error of the linear solution

To demonstrate the efficacy of the blending approach across all boundaries, the different cases have been simulated. Figure 9 contains the results for the case when the subsonic to nozzle choked boundary is crossed, whereas Figure 10 relates to the case where the nozzle-choked to turbine choked boundary comes into play.

The results in Figure 9 correspond to a 5% increase in inlet pressure ratio and a 2% decrease in the nozzle exit area. In the context of a control system, these changes would occur in a single time-step and hence represent a large gradient in the control input. It is emphasized that this rate is expected to be an upper bound on realistic control changes. In this case, the error in turbine work and mass flow rate as predicted by the unblended linear system is relatively low. The blended output offers a minimal improvement over the baseline approach. However, exit velocity predicted by the single linear system is very inaccurate, with a nearly 300% relative error. This is perhaps expected, as the underlying change in the physical behavior is directly related to the nozzle getting choked. It is interesting to note that the blended estimate of exit velocity is almost identical to the true value.

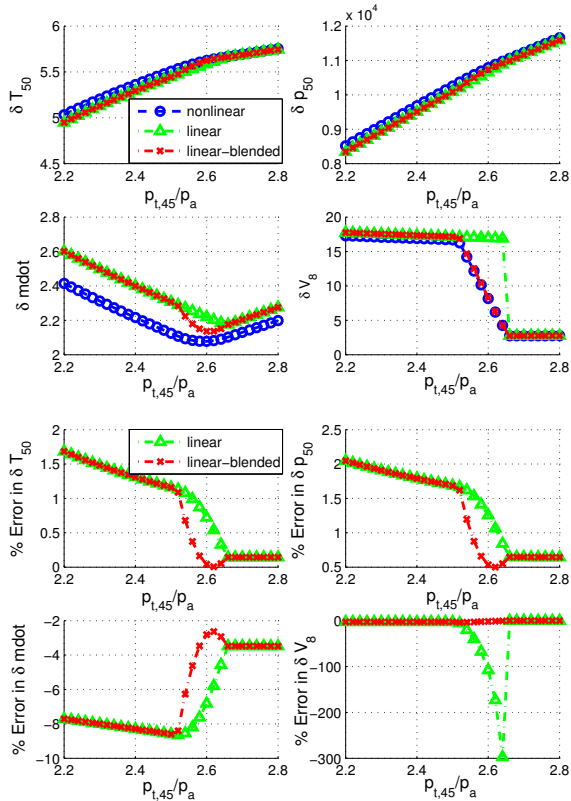


Figure 9. (a) Linear vs. nonlinear solution going from the subsonic regime to the nozzle choked regime (b) % error of the linear solution

The results in Figure 10 have been obtained by applying a 2% change in the nozzle exit area as the system sweeps over a range of pressure ratios. The blended estimates for this case offer a significant improvement in all the four outputs in the vicinity of the underlying boundary.

In all the results presented, it may be observed that the error in the linear estimates away from the subspace boundaries is generally lower when either of the two components is choked. This is consistent with the essentially linear behavior of the system when either the turbine or the nozzle is choked.

CONCLUSION

Control synthesis and stability analysis technologies are grounded in linear system theory. A detailed engine model is usually linearized via numerical perturbation methods. In this paper, an alternate approach that involves the development of physics based simplified/reduced order models followed by analytical linearization of the resulting nonlinear system has been investigated. The proposed approach has been applied to the backend of a turbine engine, i.e. a turbine nozzle system driven by high pressure air. It is proposed that, for the present purpose, a turbine can be modeled as a combination of a convergent-divergent nozzle coupled with a work extraction plane.

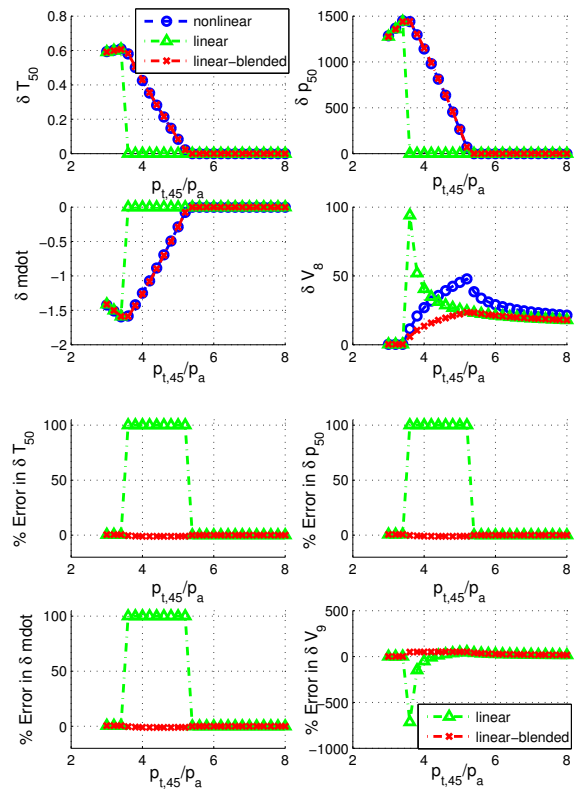


Figure 10. (a) Linear vs. nonlinear solution going from the nozzle choked regime to the turbine choked regime (b) % error of the linear solution

The simulation results of the nonlinear model highlight the key control issues of the system. The operating envelope is divided into subspaces with different flow features. More significantly, the transition from one subspace to another, while continuous, is not smooth. This leads to large errors in the linear estimates of the system outputs. However, a novel blending algorithm which can be efficiently implemented can significantly improve on the baseline estimates. In general, it may be noted that analytical linearization technique could provide a superior framework for model based control.

Two key requirements of the proposed methodology are as follows: 1) a simplified model that can be expressed analytically, and 2) the ability to capture the boundaries between discrete subspaces in an analytical form.

This paper lays out the foundation of a physics based analytical linearization technique that shows promise towards the development of physics based linear engine models. As the eventual goal is to adapt the proposed methodology in a dynamic model, the methodology will be extended to include the compressor and combustor components. The coupling with a dynamic model of the shaft speeds merits further investigation.

ACKNOWLEDGEMENT

This research is supported by Pratt & Whitney.

REFERNECE

- [1] Kulikov G. G., and Thompson H. A., 2004, Dynamic modelling of gas turbines: identification, simulation, condition monitoring, and optimal control, Springer, London.
- [2] Merrill W., Lehtinen B., and Zeller J., 1984, "The role of modern control theory in the design of controls for aircraft turbine engines," *Journal of Guidance, Control, and Dynamics*, **7**(6), pp. 652-61.
- [3] Lietzau K., and Kreiner A., 2001, "Model Based Control Concepts for Jet Engines," In Proceedings of the ASME TURBO EXPO 2001, 2001-GT-0016.
- [4] Richter H., Singaraju A., and Litt J., 2008, "Multiplexed predictive control of a large commercial turbofan engine," *Journal of Guidance, Control, and Dynamics*, **31**(2), pp. 273-81.
- [5] Simon D., and Simon D., 2005, "Aircraft turbofan engine health estimation using constrained Kalman filtering," *Transactions of the ASME. Journal of Engineering for Gas Turbines and Power*, **127**(2), pp. 323-8.
- [6] Litt J., 2008, "An optimal orthogonal decomposition method for Kalman filter-based turbofan engine thrust estimation," *Journal of Engineering for Gas Turbines and Power*, **130**(1), pp. 011601-1.
- [7] Curry T., and Behbahani A., 2004, "Propulsion directorate/control and engine health management (CEHM): real-time turbofan engine simulation," In Proceedings of the 2004 IEEE Aerospace Conference, Vol.5, pp. 3414-23.
- [8] Kim S., Ellis S., and Challener M., 2006, "Real-time engine modelling of a three shafts turbofan engine: From sub-idle to Max power rate," In Proceedings of the ASME TURBO EXPO 2006, GT2006-90656.
- [9] Stamatis A., Mathioudakis K., Ruiz J., and Curnock B., 2001, "Real Time Engine Model Implementation for Adaptive Control & Performance Monitoring of Large Civil Turbofans," In Proceedings of the ASME TURBO EXPO 2001, 2001-GT-0362.
- [10] Jaw L. C., 2009, *Aircraft engine controls : design, system analysis, and health monitoring*, AIAA, Reston.
- [11] Henrion D., Reberga L., Bernussou J., and Vary F., 2004, "Linearization and Identification of Aircraft Turbofan Engine Models," *Proceedings of the IFAC Symposium on Automatic Control in Aerospace*.
- [12] Kumar A., and Viassolo D., 2008, *Model-Based Fault Tolerant Control*.
- [13] Camporeale S., Fortunato B., and Mastrovito M., 2006, "A modular code for real time dynamic simulation of gas turbines in simulink," *Journal of Engineering for Gas Turbines and Power*, **128**(3), pp. 506-517.
- [14] Rahman N. U., and Whidborne J. F., 2009, "Real-time transient three spool turbofan engine simulation: A hybrid approach," *Journal of Engineering for Gas Turbines and Power*, **131**(5), pp. 1-8.
- [15] Mattingly J. D., 1996, *Elements of gas turbine propulsion*, McGraw-Hill, New York.
- [16] Wolodkin G., Balas G. J., and Garrard W. L., 1999, "Application of parameter-dependent robust control synthesis to turbofan engines," *Journal of Guidance, Control, and Dynamics*, **22**(6), pp. 833-838.
- [17] Balas G., 2002, "Linear, parameter-varying control and its application to a turbofan engine," *International Journal of Robust and Nonlinear Control*, **12**(9), pp. 763-96.

APPENDIX A: List of Equations

Nonlinear Equations

Turbine equations (Subsonic)

$$T_{t,45} = T_{t,5} + \frac{K\omega r}{c_p} u_{48}$$

$$T_{t,5} = T_5 + \frac{u_5^2}{2c_p}$$

$$\left(\frac{T_{t,5}}{T_5}\right)^{\frac{\gamma}{\gamma-1}} = \left(\frac{p_{t,5}}{p_5}\right)$$

$$\left(\frac{p_{t,5}}{p_{t,45}}\right) = \left[1 - \frac{1}{\eta_1} \left(1 - \frac{T_{t,5}}{T_{t,45}}\right)\right]^{\frac{\gamma}{\gamma-1}}$$

$$T_{t,45} = T_{48} + \frac{u_{48}^2}{2c_p}$$

$$\dot{m} = \rho_{48} A_{48} u_{48} = \rho_{50} A_{50} u_{50}$$

$$\left(\frac{T_{t,45}}{T_{48}}\right)^{\frac{\gamma}{\gamma-1}} = \left(\frac{p_{t,45}}{p_{48}}\right)$$

$$\dot{m} = \rho_5 A_5 u_5 = \rho_8 A_8 u_8$$

Turbine equations (choked)

$$u_{47} = \sqrt{\frac{2\gamma R T_{t,5}}{\gamma + 1}}$$

$$\dot{m} = \frac{A_{47} p_{t,45} \sqrt{\gamma}}{\sqrt{R T_{t,45}}} \left(\frac{\gamma + 1}{2}\right)^{\frac{\gamma+1}{2(\gamma-1)}}$$

Nozzle equations (subsonic)

$$u_8 = f = \frac{\dot{m}}{A_8 \rho_{t,8}} \left[1 + \frac{\gamma - 1}{2} \frac{u_8^2}{\gamma R \left(T_{t,5} - \frac{u_8^2}{2c_p} \right)} \right]^{\frac{-1}{\gamma-1}}$$

Nozzle equations (choked)

$$u_8 = \sqrt{\frac{2R\gamma T_{t,5}}{\gamma + 1}} = \frac{\dot{m} R T_{t,5}}{p_{t,5} A_8} \left(\frac{2}{\gamma + 1}\right)^{\frac{1}{\gamma-1}}$$

Linear Equations

$$\delta T_{t,45} = \delta T_{t,5} + \frac{K\omega r}{c_p} \delta u_{48}$$

$$\delta T_{t,5} = \delta T_5 + \frac{u_5}{c_p} \delta u_5$$

$$\frac{\gamma}{\gamma-1} \left(\frac{T_{t,5}}{T_5}\right)^{\frac{1}{\gamma-1}} \frac{1}{T_5} \delta T_{t,5} - \frac{1}{p_5} \delta p_{t,5} - \frac{\gamma}{\gamma-1} \left(\frac{T_{t,5}}{T_5}\right)^{\frac{\gamma}{\gamma-1}} \frac{1}{T_5} \delta T_5 + \left(\frac{p_{t,5}}{p_5^2}\right) \delta p_5 = 0$$

$$\frac{\gamma}{\gamma-1} \left[1 - \frac{1}{\eta} \left(1 - \frac{T_{t,5}}{T_{t,45}} \right) \right]^{\frac{1}{\gamma-1}} \left[\frac{1}{\eta T_{t,45}} \delta T_{t,5} - \frac{T_{t,5}}{\eta T_{t,45}^2} \delta T_{t,45} \right] - \frac{1}{p_{t,45}} \delta p_{t,5} + \left(\frac{p_{t,5}}{p_{t,45}^2} \right) \delta p_{t,45} = 0$$

$$\delta T_{t,45} = \delta T_{48} + \frac{u_{48}}{c_p} \delta u_{48}$$

$$\frac{\delta p_{48}}{p_{48}} - \frac{\delta T_{48}}{T_{48}} + \frac{\delta u_{48}}{u_{48}} - \frac{\delta p_5}{p_5} + \frac{\delta T_5}{T_5} - \frac{\delta u_5}{u_5} = 0$$

$$\frac{\gamma}{\gamma-1} \left(\frac{T_{t,45}}{T_{48}} \right)^{\frac{1}{\gamma-1}} \frac{1}{T_{48}} \delta T_{t,45} - \frac{1}{p_{48}} \delta p_{t,45} - \frac{\gamma}{\gamma-1} \left(\frac{T_{t,45}}{T_{48}} \right)^{\frac{\gamma}{\gamma-1}} \frac{1}{T_{48}} \delta T_{48} + \left(\frac{p_{t,45}}{p_{48}^2} \right) \delta p_{48} = 0$$

$$\frac{\delta p_5}{p_5} - \frac{\delta T_5}{T_5} + \frac{\delta u_5}{u_5} - \frac{\delta p_8}{p_8} + \frac{\delta T_8}{T_8} - \frac{\delta A_8}{A_8} = \frac{c_p (\delta T_{t,5} - \delta T_8)}{u_8^2}$$

With following variations

When flow is subsonic

$$\delta p_8 = 0$$

$$\delta T_8 = \delta T_{t,5} \left(\frac{p_8}{p_{t,5}} \right)^{\frac{\gamma-1}{\gamma}} + T_{t,5} \left(\frac{\gamma-1}{\gamma} \right) \left(\frac{p_8}{p_{t,5}} \right)^{\frac{\gamma-1}{\gamma}} \frac{1}{p_{t,5}} \delta p_{t,5}$$

$$\delta \dot{m} = \frac{p_{48}}{RT_{48}} \left(\frac{\delta p_{48}}{p_{48}} - \frac{\delta T_{48}}{T_{48}} \right) A_{48} u_{48} + \frac{p_{48}}{RT_{48}} \delta A_{48} u_{48} + \frac{p_{48}}{RT_{48}} A_{48} \delta u_{48}$$

$$\delta u_8 = \frac{\frac{\partial f}{\partial p_{t,5}} \delta p_{t,5} + \frac{\partial f}{\partial T_{t,5}} \delta T_{t,5}}{1 - \frac{\partial f}{\partial u_8}}$$

When nozzle is choked

$$\delta p_8 = \delta p_{t,5} \left(\frac{2}{\gamma+1} \right)^{\frac{\gamma}{\gamma-1}}$$

$$\delta T_8 = \delta T_{t,5} \left(\frac{2}{\gamma+1} \right)$$

$$\delta \dot{m} = \frac{p_{48}}{RT_{48}} \left(\frac{\delta p_{48}}{p_{48}} - \frac{\delta T_{48}}{T_{48}} \right) A_{48} u_{48} + \frac{p_{48}}{RT_{48}} \delta A_{48} u_{48} + \frac{p_{48}}{RT_{48}} A_{48} \delta u_{48}$$

$$\delta u_8 = \sqrt{\frac{R\gamma}{2(\gamma+1)T_{t,5}}} \delta T_{t,5}$$

When turbine is choked

$$\delta \dot{m} = \frac{\sqrt{\gamma} A_{47}}{\sqrt{RT_{t,45}}} \left(\frac{\gamma+1}{2} \right)^{\frac{\gamma+1}{2(\gamma-1)}} \delta p_{t,45} - \frac{p_{t,45} \sqrt{\gamma} A_{47}}{2\sqrt{RT_{t,45}^{3/2}}} \left(\frac{\gamma+1}{2} \right)^{\frac{\gamma+1}{2(\gamma-1)}} \delta T_{t,45}$$

$$\delta u_8 = \frac{\frac{\partial f}{\partial p_{t,5}} \delta p_{t,5} + \frac{\partial f}{\partial T_{t,5}} \delta T_{t,5}}{1 - \frac{\partial f}{\partial u_8}}$$